Available online at www.sciencedirect.com

ScienceDirect

Proceedings of the Combustion Institute 39 (2023) 2575–2586

Proceedings of the Combustion Institute

www.elsevier.com/locate/proci

Inertial effects on the interaction of water droplets with turbulent premixed flames: A direct numerical simulation analysis

Josef Hasslberger [a,1,*], Riccardo Concetti [a], Nilanjan Chakraborty [b], Markus Klein [a]

[a] *Department of Aerospace Engineering, University of the Bundeswehr Munich, Werner-Heisenberg-Weg 39, Neubiberg 85577, Germany*

[b] *School of Engineering, Newcastle University, Claremont Road, Newcastle NE1 7RU, UK*

Received 4 January 2022; accepted 6 July 2022
Available online 20 August 2022

Abstract

The effects of droplet inertia on the reaction zone structure, overall burning rate, and flame surface area during interaction of water droplets with a statistically planar turbulent premixed stoichiometric n-heptane-air flame based on three-dimensional carrier phase Direct Numerical Simulations have been analysed. Different initially mono-sized droplets are considered for this study in order to analyse the inertial effects for different droplet sizes. Droplet inertia has been demonstrated to have an important influence on the extent of evaporation of water droplets and water vapour concentration arising from evaporation within the flame. It has been found that the residence time of droplets within the flame increases due to droplet inertia and therefore the evaporation and the cooling effect associated with the extraction of latent heat are stronger for inertial droplets than in the case of hypothetical inertialess droplets. The stronger cooling effects for inertial droplets lead to smaller burned gas temperature and thicker flame than the corresponding cases with inertialess droplets. The aforementioned cooling effect induced by latent heat of evaporation of water droplets reduces the burning rate and the likelihood of obtaining high gradient magnitudes of reaction progress variable and temperature within the flame for the cases with water droplets in comparison to the corresponding purely gaseous turbulent premixed flames, and this tendency is stronger for inertial droplets. The stronger cooling effect, along with the reduction of reactant concentrations within the flame due to greater extent of evaporation for inertial droplets, gives rise to a smaller extent of flame area generation and overall burning rate than in the corresponding cases with inertialess droplets. It has been found that water droplet inertia acts to reduce the burning rate and the consumption rate of reactants per unit flame surface area during

* Corresponding author.
E-mail address: josef.hasslberger@unibw.de (J. Hasslberger).

[1] No figure needs to be printed in colour in the hard copy. All figures need to be printed in colour in the online version.

https://doi.org/10.1016/j.proci.2022.07.039

the interaction of water droplets with turbulent premixed flames within the parameter range analysed in this paper.

Keywords: Inertial effects; Flame propagation; Water droplet diameter; Turbulence intensity; Premixed flames

1. Introduction

Water injection in combustion systems has been in use for a long time in car engines (e.g., BMW M4 GTS engine, WaterBoost system by Bosch) and gas turbines [1]. The interaction of water droplets with a flame is also important from the point of view of fire suppression [2] and explosion mitigation [3]. The water droplet size distribution and the flame-droplet interaction can have a significant influence on the overall burning rate [3]. It has been demonstrated that the interaction of water droplets with the flame surface could potentially affect the turbulence level within the flame brush and thereby influence the turbulent burning velocity [4]. Previous fully resolved two-dimensional simulations [5] demonstrated that in addition to the droplet sizes, the distance between the droplets could also affect the rate of flame propagation. The present authors recently carried out three-dimensional carrier phase simple chemistry Direct Numerical Simulations (DNS) of the interaction of water droplets with n-heptane-air turbulent premixed flames for different turbulence intensities, droplet loading and droplet diameters and revealed that the droplet size affects the overall burning rate in a non-linear manner [6]. They also revealed that the cooling effect associated with the evaporation of droplets dominates over the changes in the concentration of reactants in the gaseous phase [6]. The cooling effects due to the presence of droplets induce weaker thermal expansion effects and a smaller overall burning rate than in purely gaseous turbulent premixed flames [6]. Numerical experiments were conducted by Hasslberger et al. [6] to demonstrate the effects of latent heat on the overall burning rate and turbulence level within the flame brush. Based on this analysis, Hasslberger et al. [6] also proposed a reduced-order model for the effects of cooling and dilution induced by water droplets on the laminar burning velocity by considering the time scales of droplet evaporation and residence time within the flame [6]. This analysis [6] suggests that the inertial effects of the water droplets could potentially play a key role in determining the overall burning rate and turbulence burning velocity. It was discussed in several previous analytical [7–9], experimental [10,11] and numerical [12] studies that the inertia of fuel droplets could affect the gaseous phase reacting mixture composition, and thereby the overall burning rate in fuel droplet-laden mixtures. A recent carrier phase DNS analysis [12] of spherically expanding flames of n-heptane droplets revealed that the droplet concentration within the flame increases due to droplet inertia, which, in turn, increases the gaseous phase equivalence ratio and overall burning rate in agreement with previous experimental findings by Lawes and Saat [11]. A thorough understanding of the effects of droplet inertia enables the development of high-fidelity multiphase flow models, but this goal is made considerably demanding in reacting flows because of the influence of the inertial effects on the flame propagation and burning rate. There is no straightforward way to assess the implications of accurate representation of inertial effects on the flame physics without a numerical experiment that considers inertialess droplets (as a limiting physical scenario) and compares the results for hypothetical droplet cases with the corresponding results with actual inertial droplets. This cannot be done in experiments, but it is a standard numerical and analytical technique to consider hypothetical conditions to analyse a physical phenomenon in isolation. The same approach was adopted previously in Ref. [12] to analyse the inertial effects of fuel droplets but to the best of the authors' knowledge, there is no analysis in the existing literature on the roles of droplet inertia on the water droplet-premixed flame interaction under turbulent conditions. This paper addresses this gap in the existing literature by carrying out numerical experiments using carrier phase DNS involving hypothetical inertialess droplets with the properties of water for comparison of the combustion characteristics to the corresponding cases involving interactions of inertial water droplets with a stoichiometric turbulent premixed n-heptane flame. In this respect, the main objectives of the current analysis are: (a) to demonstrate the effects of droplet inertia on flame surface area and overall burning rate during the interaction of water droplets with turbulent premixed flames, and (b) to provide physical explanations for the observed differences between inertial and inertialess droplet cases.

2. Mathematical background and numerical implementation

A modified single-step irreversible chemical reaction [13], for which the activation energy and

heat of combustion are taken to be functions of the gaseous equivalence ratio, is considered for this analysis for the purpose of the computational economy in the interest of an extensive parametric analysis (e.g. 3 different droplet diameters and two different turbulence intensities for both inertial and inertialess droplets. Note, that Ref. [6] dealt only with inertial droplets for a smaller range of turbulence intensity than considered in this analysis). It has been shown elsewhere [14] that this methodology captures the unstrained laminar burning velocity $S_{b(\phi)}$ variation with gaseous phase equivalence ratio ϕ_g obtained from detailed chemistry simulations [15]. Moreover, this chemical mechanism has also been shown elsewhere [6] to capture the laminar burning velocity $S_{b(\phi)}$ variation with water vapour concentration Y_W^g in the unburned gas for the range of Y_W^g encountered in the current analysis. All gaseous species are assumed to have Lewis numbers of unity and standard values are adopted for the ratio of specific heats ($\gamma = 1.4$) and Prandtl number ($Pr = 0.70$). The spherical water droplets are assumed to interact with an initially stoichiometric (i.e. $\phi_g = 1.0$) n-heptane-air premixed flame. For the current analysis, the gaseous phase is considered in terms of an Eulerian formulation, whereas liquid water droplets are individually tracked in a Lagrangian sense. The quantities transported for each droplet (subscript d is used for droplet quantities) are formulated in the following manner [6,14,16,17]:

$$\begin{aligned} &\frac{d\vec{x}_d}{dt} = \vec{u}_d;\ \frac{d\vec{u}_d}{dt} = \frac{\vec{u}(\vec{x}_d,t)-\vec{u}_d}{\tau_d^u};\ \frac{da_d^2}{dt} = -\frac{a_d^2}{\tau_d^p};\\ &\frac{dT_d}{dt} = \frac{\hat{T}(\vec{x}_d,t)-T_d-B_d L_v/C_p^g}{\tau_d^T} \end{aligned} \tag{1}$$

Here, $\vec{x}_d, \vec{u}_d, a_d, T_d$ are the position vector, velocity vector, droplet diameter and temperature of individual droplets, $\vec{u}$ and $\hat{T}$ are gaseous phase velocity vector and temperature, respectively, L_v is the latent heat of vaporization, and relaxation timescales for droplet velocity, τ_d^u diameter τ_d^p and temperature τ_d^T are given by: $\tau_d^u = \rho_d a_d^2/(18C_u\mu)$; $\tau_d^p = \left(\rho_d a_d^2/4\mu\right)(Sc/Sh_c)/\log(1+B_d)$ and $\tau_d^T = \left(\rho_d a_d^2/6\mu\right)(Pr/Nu_c)[B_d/\log(1+B_d)]C_p^l/C_p^g$, respectively. Here, ρ_d is the droplet density, Sc stands for the Schmidt number, C_p^l denotes the specific heat for the liquid phase, $C_u = 1 + Re_d^{2/3}/6$ is the corrected drag coefficient, Re_d is the droplet Reynolds number, B_d is the Spalding number, Sh_c and Nu_c are the corrected Sherwood and Nusselt numbers, respectively, which are expressed as [6,14,16,17]:

$$\begin{aligned} &Re_d = \frac{\rho|\vec{u}(\vec{x}_d,t)-\vec{u}_d|a_d}{\mu};\\ &B_d = \frac{Y_W^S - Y_W^g(\vec{x}_d,t)}{1-Y_W^S};\\ &Sh_c = Nu_c = 2 + \frac{0.555 Re_d Sc}{\left(1.232+Re_d Sc^{4/3}\right)^{1/2}} \end{aligned} \tag{2}$$

where Y_W^S is the water vapour mass fraction Y_W^g at the droplet surface. The partial pressure of the water vapour at the droplet surface p_F^s is evaluated based on the Clausius–Clapeyron equation [6,14,16,17]: $p_W^s = p_{ref}\exp\left(L_v/R\left[\left(1/T_{ref}^S\right) - \left(1/T_d^s\right)\right]\right)$ and $Y_W^S = (1+\left(W_g/W_W\right)\left[p(\vec{x}_d,t)/p_W^s - 1\right])^{-1}$ where T_{ref}^S represents the boiling point of water at a pressure p_{ref}, T_d^S is assumed to be T_d, and W_g and W_W are the molecular weights of the gaseous mixture and water vapour, respectively. In order to analyse the influence of droplet inertia, hypothetical simulations have been conducted for inertialess droplets, which follow $d\vec{x}_d/dt = \vec{u}$, and $d\vec{u}_d/dt$ becomes irrelevant, but the rest of the expressions in Eq. (1) are kept unchanged.

For the present analysis, DNS of statistically planar turbulent flames are carried out for different initial values of the normalised root-mean-square turbulent velocity of $u'/S_{b(\phi_g=1)}$ with a non-dimensional longitudinal integral length-scale of $L_{11}/\delta_{st} = 2.5$ where $\delta_{st} = \left(T_{ad(\phi_g=1)} - T_0\right)/max|\nabla\hat{T}|_L$ is the thermal flame thickness of the stoichiometric mixture with $\hat{T}$, $T_{ad(\phi_g=1)}$ and T_0 being the instantaneous dimensional temperature, stoichiometric adiabatic flame temperature and unburned gas temperature, respectively. The heat release parameter $\tau = \left(T_{ad(\phi_g=1)} - T_0\right)/T_0$ is taken to be 6.54, which corresponds to an unburned gas temperature of 300K under atmospheric pressure because thermochemical data for n-heptane is well-documented for the atmospheric pressure. Moreover, in the context of fire suppression and explosion mitigation, it is worth noting that usually accidents occur as well at ambient conditions. Additional simulations have been carried out also for fully gaseous phase stoichiometric turbulent premixed n-heptane-air flames for the sake of comparison with the corresponding cases with water droplets. A well-known DNS code SENGA+ [6,14,17], which solves the conservation equations of mass, momentum, energy and species in non dimensional form has been used for the present analysis. In SENGA+, high order finite difference (10^{th} order central difference for the internal grid points with a gradual decrease in the order of accuracy to a 2^{nd} order one-sided scheme at the non-periodic boundaries) and Runge-Kutta (3^{rd} order low-storage) schemes are employed. For this analysis, the simulation domain is taken to be $30\delta_{st} \times 20\delta_{st} \times 20\delta_{st}$ which is discretised by a uniform Cartesian grid of $384 \times 256 \times 256$. This grid ensures 10 grid points are kept within δ_{st} and the Kolmogorov length scale η is also resolved. The long side of the simulation domain is aligned to the mean direction of flame propagation (i.e. x direc-

tion in this configuration) and boundaries in this direction are taken to be partially non-reflecting, which are specified using the Navier-Stokes Characteristic Boundary Conditions technique. The transverse boundaries in y and z directions are considered to be periodic. Three different initially mono-sized water droplets (i.e. $a_d/\delta_{st} = 0.02$, 0.04 and 0.06, which correspond to a range of 10–30μm) have been considered for each turbulence intensity for a water loading of $Y_W = 0.1$ where $Y_W = Y_W^l + Y_W^g = m_W/(m_W + m_0)$ is the mass fraction of water (in both liquid (l)+gaseous (g) phases) in the unburned gas (and thus independent of the chemical reaction) with m_W being the total amount of water injected in a combined mass of air and fuel mixture given by m_0. The parameters chosen for this analysis are representative of previous experiments [1,2]. The Stokes number for the inertial droplets can be defined as $St = \tau_p u'/L_{11} = \rho_d a_d^2 u'/(18 C_u \mu L_{11})$ (where L_{11}/u' is the turbulent time scale) and it remains smaller than 0.14 (0.28) for the largest droplet in the turbulent cases with $u'/S_{b(\phi_g=1)} = 4.0$ (8.0). Alternatively, the Stokes number $St' = \tau_p S_{b(\phi_g=1)}^2/\alpha_{T0} = \rho_d a_d^2 S_{b(\phi_g=1)}^2/(18 C_u \mu \alpha_{T0})$ can be calculated based on the chemical timescale $\alpha_{T0}/S_{b(\phi_g=1)}^2$ and the maximum value of St' remains smaller than 0.44 for the largest droplets considered here where α_{T0} is the thermal diffusivity of the unburned gas. For the aforementioned values of the Stokes number, there is a lag between the droplet motion and the background fluid motion due to the drag experienced by the inertial droplets. The initial droplet number density ρ_N varies between $1.14 \leq (\rho_N)^{1/3}\delta_{st} \leq 3.41$ in the unburned gas depending on the value of a_d considered here, and the liquid volume fraction remains well below 0.02%. The ratio a_d/η is 0.06, 0.12 and 0.18 (0.1, 0.2 and 0.3) for a_d/δ_{st} =0.02, 0.04 and 0.06, respectively for $u'/S_{b(\phi_g=1)} = 4.0$ (8.0), and the mean normalised inter-droplet distance s_d/η ranges between 1.45 and 4.35. The ratio of the initial droplet volume to the computational cell volume V_d/V_{cell} is 0.007, 0.057 and 0.191 for $a_d/\delta_{st} = 0.02$, 0.04 and 0.06, respectively, which is comparable to several previous analyses [6,17,18], and justifies the point source assumption.

The generic governing equations for the carrier phase can be expressed as [6,14,16,17]:

$$\frac{\partial \rho\varphi}{\partial t} + \frac{\partial \left(\rho u_j \varphi\right)}{\partial x_j} = \frac{\partial}{\partial x_j}\left(R_\varphi \frac{\partial \varphi_1}{\partial x_j}\right) + \dot{\omega}_\varphi + \dot{S}_\varphi + \dot{S}_g \tag{3}$$

Here, $\varphi = \{1, u_i, e, Y_F, Y_O, Y_W^g\}$ and $\varphi_1 = \{1, u_i, T, Y_F, Y_O, Y_W^g\}$ for the conservation equations of mass, momentum, energy, and mass fractions, respectively. In Eq. (3), $R_\varphi = \rho\nu/\sigma_\varphi$ for $\varphi = \{1, u_i, Y_F, Y_O, Y_W^g\}$) and $R_\varphi = \lambda$ for $\varphi = e$, respectively, where $e = \int_{T_{ref}}^{T} C_V dT + u_i u_i/2$ is the specific stagnation internal energy with T_{ref} and C_V being the reference temperature and specific heat at constant volume, respectively. The $\dot{\omega}_\varphi$ term in Eq. (3) refers to reaction rate, $\dot{S}_g$ stands for an appropriate source/sink term in the gaseous phase (e.g. pressure forces in the momentum equation) and $\dot{S}_\varphi = -(1/V_{cell})\Sigma_d d(m_d\varphi_d)/dt$ is the appropriate term due to droplet evaporation and is responsible for two-way coupling where $m_d = \rho_d(1/6)\pi a_d^3$ is the droplet mass. Other variables are ν, kinematic viscosity, λ, thermal conductivity and σ_φ, an appropriate Schmidt number corresponding to φ.

The extent of the completion of the chemical reaction can be quantified with the help of a reaction progress variable c, which increases monotonically from 0 in the unburned gas to 1.0 in the fully burned gas. The reaction progress variable c is defined here based on oxygen mass fraction, Y_O and mixture fraction, $\xi = (Y_F - Y_O/s + Y_{O\infty}/s)/(Y_{F\infty} + Y_{O\infty}/s)$ in the following manner [6,14,16,17]:

$$c = \frac{Y_{O\infty}(1-\xi) - Y_O}{Y_{O\infty}(1-\xi) - max(0, \{\xi_{st} - \xi\}/\xi_{st})Y_{O\infty}} \tag{4}$$

where $Y_{O\infty} = 0.233$ is the oxygen mass fraction in air and $Y_{F\infty} = 1.0$ is the fuel mass fraction in the pure fuel stream. For n-heptane, C_7H_{16}, $s = 3.52$ is the stoichiometric mass ratio of oxidiser to fuel and $Y_{F_{st}} = 0.0621$ and $\xi_{st} = 0.0621$ are the corresponding stoichiometric fuel mass fraction and mixture fraction, respectively.

A standard pseudo-spectral method has been used to initialise turbulent velocity fluctuations by an incompressible homogeneous isotropic velocity field. The flame-turbulence interaction takes place under decaying turbulence and statistics are taken at $3.0t_{chem} = 3.0\alpha_{T0}/S_{b(\phi_g=1)}^2$. Note that $t_{chem} = 0.815L_{11}/u'$ and $1.63L_{11}/u'$ for initial $u'/S_{b(\phi_g=1)} = 4.0$ and 8.0 cases, respectively. This simulation time remains comparable to several previous analyses [6,17,18] and by this time both the volume-integrated burning rate and flame surface area reached a quasi-stationary state and were not changing appreciably with time for the cases considered here (see [6] exemplarily for inertial droplet cases).

3. Results and discussion

The distributions of non-dimensional temperature $T = (\hat{T} - T_0)/(T_{ad(\phi_g=1)} - T_0)$ and the mass fraction of the evaporated water vapour in the gaseous phase (excluding the product water mass fraction) Y_W^g in the central midplane along with the droplets residing in that plane at the time when statistics are extracted, are presented in Fig. 1 for

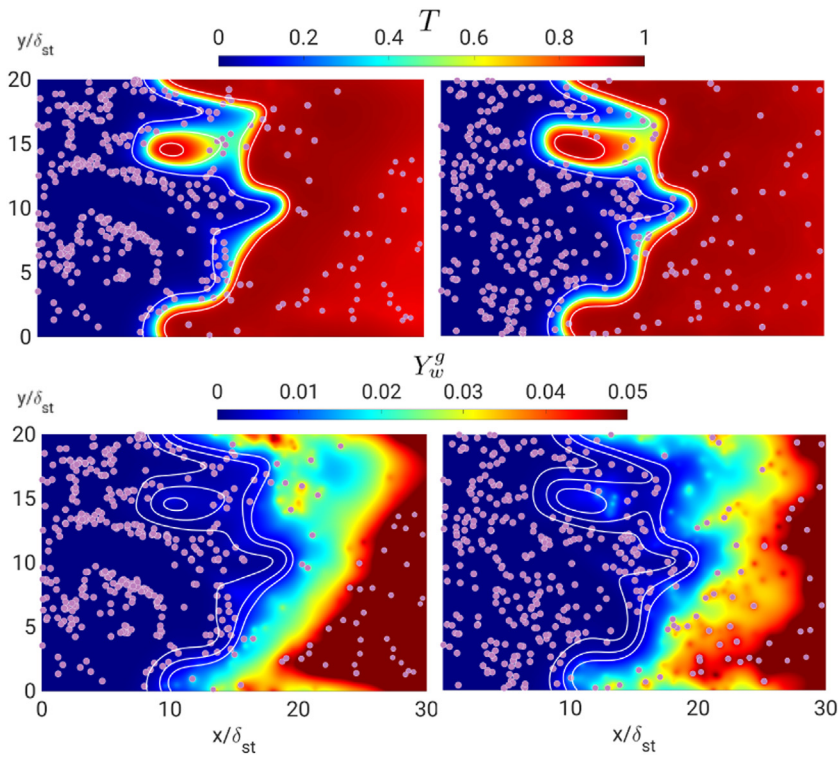

Fig. 1. Distribution of T (1^{st} row) and Y_W^g (2^{nd} row) (white lines show $c = 0.1$, 0.5 and 0.9 contours from left to right) and on the central $x - y$ mid-plane for flames with initial $u'/S_{b(\phi_g=1)} = 4.0$ for inertial (1^{st} column) and inertialess (2nd column) droplet cases with initial $a_d/\delta_{st} = 0.04$ at $t/t_{chem} = 4$. Pink dots show the droplets residing on the plane (not to the scale).

both inertial and inertialess droplets. The three-dimensional instantaneous views of $c = 0.95$ and $T = 0.95$ iso-surfaces for a representative case with inertial particles are shown in Fig. 2. It can be seen from Fig. 2 that the $c = 0.95$ and $T = 0.95$ iso-surfaces are not coincident with each other, and $T = 0.95$ occurs in the downstream of $c = 0.95$ in the mean flow direction. Therefore, the droplet density behind $c = 0.95$ isosurface is greater than that in the case of the $T = 0.95$ iso-surface.

It can be seen from Figs. 1 and 2 that the water droplets do not evaporate completely within the flame due to high latent heat of water (~ 7.16 times of the latent heat of n-heptane). Even for the smallest droplet size, where the evaporation is the highest, the maximum value of Y_W^g remains below 0.1 within the flame (i.e. $0.01 < c < 0.99$) despite the water loading of the unburned gas of $Y_W = 0.1$ [6]. Therefore, water injection does not significantly affect the chemical processes within the flame for the cases considered here. Due to the slow evaporation, water droplets do not significantly deform the reaction progress variable c iso-surfaces, but they distort the non-dimensional temperature T iso-surfaces due to the extraction of the latent heat of evaporation [6] (cf. Fig. 2). This behaviour, which also holds for initial $u'/S_{b(\phi_g=1)} = 8.0$ cases, is similar for both inertialess and inertial droplets. A comparison between T and Y_W^g fields of inertial and inertialess particles reveals that the inertial droplets show clustering in the unburned gas (i.e. $T = 0$), whereas no such clustering is observed for the inertialess droplets. This is consistent with previous findings [19] that inertial particles tend to cluster in the high strain rate and low vorticity regions. This behavior can be confirmed from Fig. 3 which shows the distribution of the coherent structure function $F_{CS} = Q/E$ with $Q = (\Omega_{ij}\Omega_{ij} - S_{ij}S_{ij})/2$ and $E = (\Omega_{ij}\Omega_{ij} + S_{ij}S_{ij})/2$, where S_{ij} and Ω_{ij} are the rate of strain tensor and rate of rotation tensor, respectively. Accordingly, F_{CS} takes values of -1 and $+1$ for pure straining and pure rotation, respectively, and is exemplarily shown for the case with initial $u'/S_{b(\phi_g=1)} = 4.0$ and $a_d/\delta_{st} = 0.04$ but the same qualitative behaviour was observed for other cases.

It can be discerned from Y_W^g fields in Fig. 1 that higher particle density, and a greater probability of obtaining high Y_W^g values in the burned gas are obtained for the inertialess particles. This can be

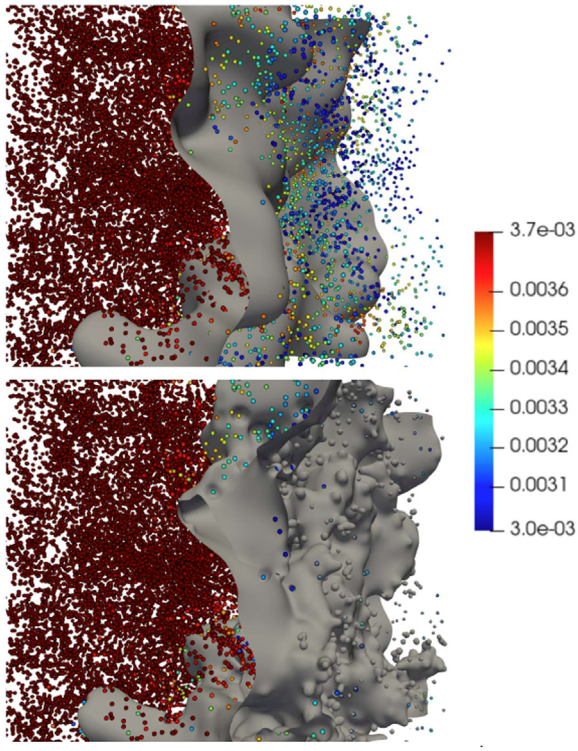

Fig. 2. Instantaneous views of $c = 0.95$ (1^{st} row) and $T = 0.95$ (2nd row) iso-surfaces (shown in grey) seen from the burned gas side for initial values of $u'/S_{b(\phi_g=1)} = 4.0$, $a_d/\delta_{st} = 0.04$, and $Y_W = 0.1$ for inertial particles at $t/t_{chem} = 2.1$. The colour of not-to-the-scale droplets indicates the instantaneous values of a_d/δ_{st}.

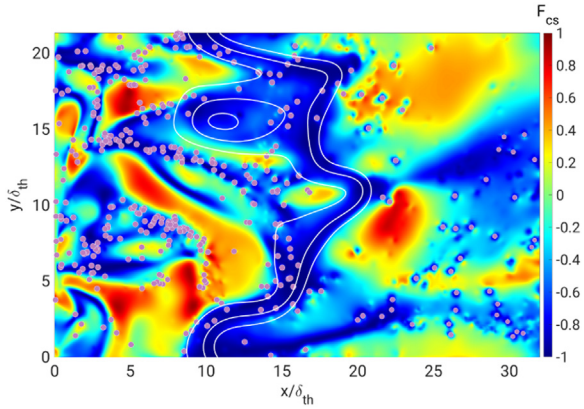

Fig. 3. Distribution of the coherent structure function F_{CS} (values of -1 and $+1$ corresponding to pure strain and pure rotation, respectively) on the central $x-y$ mid-plane for inertial droplet cases with initial $a_d/\delta_{st} = 0.04$ and initial $u'/S_{b(\phi_g=1)} = 4.0$. Pink dots show the droplets residing on the plane (not to the scale). White lines show $c = 0.1$, 0.5 and 0.9 contours from left to right.

substantiated from the variations of $\overline{Y_W^g}$ and $\overline{T}$ with x/δ_{st} shown in Fig. 4 where $\overline{Q}$ represents the ensemble-averaged values of the samples of a general quantity Q over the homogeneous directions (i.e. y and z directions in this configuration). Under the unity Lewis number, adiabatic low-Mach number condition, $\bar{c} = \tilde{T}$ is maintained for the gaseous premixed flame but it is not valid for droplet cases. However, the variation of $\bar{c}$ with x/δ_{st} remains qualitatively similar to that of $\tilde{T}$.

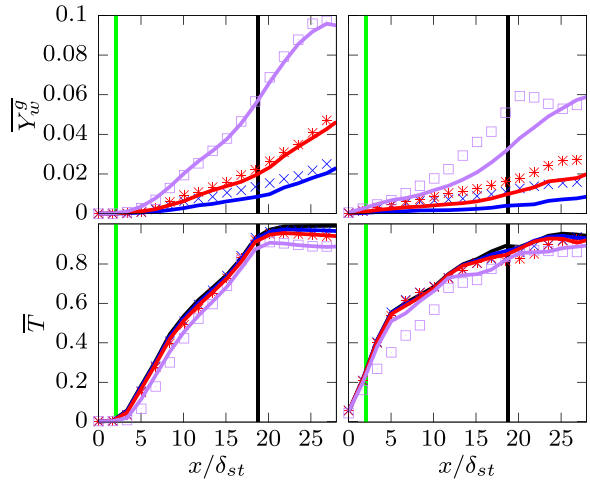

Fig. 4. Variations of $\overline{Y_W^g}$ (1^{st} row) and $\overline{T}$ (2nd row) at $t/t_{chem} = 4$, with x/δ_{st} for initial $u'/S_{b(\phi_g=1)} = 4.0$ (1^{st} column) and 8.0 (2nd column) cases with inertial (markers) and inertialess (solid line) droplet cases with initial $a_d/\delta_{st} = 0.02$ (purple), 0.04 (red), 0.06 (blue) and purely premixed conditions (black solid line). The locations corresponding to $\bar{c} = 0.05$ and $\bar{c} = 0.95$ are shown by green and black vertical lines, respectively. (For interpretation of the references to color in this figure legend, the reader is referred to the web version of this article.)

Fig. 4 shows that the maximum $\overline{T}$ value in the cases with liquid water injection with both inertial and inertialess droplets remain smaller than the maximum value of $\overline{T}$ (i.e. $\overline{T} \approx 1.0$) for the gaseous premixed flame case. This drop in the maximum values of $\overline{T}$ for the droplet cases takes place due to the smaller reactant concentrations in the unburned gas in comparison to that in the gaseous premixed flame, and also due to the cooling effect resulting from latent heat extraction of water droplets in the burned gas, with the later effect dominating over the former for the cases considered here [6]. This behaviour is particularly strong for smaller droplets (e.g. initial $a_d/\delta_{st} = 0.02$ cases) due to their greater likelihood of evaporation, whereas the maximum value of $\overline{T}$ for the large droplet cases (e.g. initial $a_d/\delta_{st} = 0.06$ cases) remain comparable to (but slightly smaller than) the corresponding value in the gaseous premixed flame case due to their smaller extent of evaporation. Recalling that $\overline{Y_W^g}$ does not include the product water mass fraction, it can be seen from Fig. 4 that $\overline{Y_W^g}$ values in the region given by $0.1 < \bar{c} < 0.9$ for inertialess particles remain mostly smaller than that for inertial particles. By contrast, $\overline{Y_W^g}$ values in the region given by $\bar{c} > 0.9$ for inertialess particles remain greater than that for inertial particles. The smaller (greater) values of $\overline{Y_W^g}$ within the region given by $0.1 < \bar{c} < 0.9$ ($\bar{c} > 0.9$) for inertialess particles are indicative of the lower particle density (therefore less evaporation of droplets) within the flame and higher particle density (consequently relatively higher amount of evaporated water vapour) in the burned gas. It has been found that the number of droplets within the zone given by $0.1 < \bar{c} < 0.9$ is −9.65%, 6.21% and 15.77% (16.16%, 44.75% and 55.56%) smaller for inertialess droplets than in the corresponding inertial droplet cases for initial $a_d/\delta_{st} = 0.02$, 0.04 and 0.06 cases with $u'/S_{b(\phi_g=1)} = 4.0$ (8.0). In statistically planar flames, the mean flow is directed from the unburned gas side to the burned gas side of the flame brush. In the case of inertialess droplets, there is no lag between the droplet and fluid velocity and as a result, the inertialess droplets more readily pass through the flame with a small residence time within the flame and thereby undergo less evaporation in this region before reaching the burned gas. The higher residence time of inertial droplets within the flame in comparison to inertialess droplets is particularly prevalent for larger droplets and higher turbulence intensity because of higher Stokes number. This effect of droplet inertia is also consistent with previous analytical [7–9] and numerical [12] findings and experimental postulation [10,11] involving fuel droplets. The increased likelihood of evaporation of inertialess droplets in the burned gas region reduces the probability of finding a lower value of T within the flame (i.e., $0.1 < c < 0.9$) in comparison to that in the case of corresponding inertial droplets. This tendency is most prominent for the smallest droplets and weakens with increasing a_d/δ_{st}, which can be substantiated from the probability density functions (PDFs) of T for $0.7 < c \leq 0.99$ shown in Fig. 5. In order to demonstrate the influence of the cooling effects induced by the evaporation of water droplets on the flame structure, the mean values of $\dot{\omega}_c \times \delta_{st}/(\rho_0 S_{b(\phi_g=1)})$ (with ρ_0 being the unburned

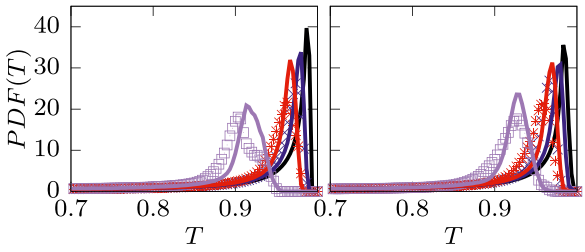

Fig. 5. *PDFs* of T in the region corresponding to $0.7 < c < 0.99$ at $t/t_{chem} = 3$. Initial $u'/S_{b(\phi_g=1)} = 4.0$ (1^{st} column) and 8.0 (2nd column) cases with inertial (markers) and inertialess (solid line) droplet cases with initial $a_d/\delta_{st} = 0.02$ (purple), 0.04 (red), 0.06 (blue) and purely premixed conditions (black solid line). (For interpretation of the references to color in this figure legend, the reader is referred to the web version of this article.)

gas density) and $|\nabla c| \times \delta_{st}$ conditional upon c are shown in Fig. 6 for both inertial and inertialess particles where $\dot{\omega}_c$ is the reaction rate of c, and is expressed as [20,21]: $\dot{\omega}_c = -\xi_{st}\dot{\omega}_O/[Y_{O\infty}\xi(1-\xi_{st})]$ for $\xi \leq \xi_{st}$ and $\dot{\omega}_c = -\dot{\omega}_O/[Y_{O\infty}(1-\xi)]$ for $\xi > \xi_{st}$ where $\dot{\omega}_O$ is the reaction rate of O_2. It is worth noting that the mean values of reaction rate magnitudes of fuel and oxidiser (i.e. $|\dot{\omega}_F|$ and $|\dot{\omega}_O|$) show qualitatively similar behaviour as that of $\dot{\omega}_c$ and thus are not explicitly shown here. Fig. 6 shows that the peak value of $\dot{\omega}_c$ for the droplet cases decreases in comparison to the corresponding value in the gaseous premixed flame, and this reduction of the peak mean value of $\dot{\omega}_c$ is the strongest for the smallest droplets considered here.

The faster evaporation for smaller water droplets reduces the mass fractions of fuel and oxidiser in the reactants and also acts to reduce the temperature due to extraction of the (large) latent heat. It was demonstrated by Hasslberger et al. [6] that the cooling effects induced by the extraction of latent heat dominate over the reduction in mass fractions of fuel and oxidiser. The reduction in $\dot{\omega}_c$ with an increase in Y_W is indicative of the reduction of the burning velocity with an increase in water droplet loading, which was demonstrated and explained by a reduced-order model by Hasslberger et al. [6], and thus is not repeated here (but see Fig. 8 later). The inverse of the peak mean value of $|\nabla c|$ can be considered to be a measure of the flame-front thickness [22] (i.e. $\delta \sim 1/\max\{|\nabla c|\}$ where $\{Q\}$ is the mean value of a general quantity of Q conditional upon c), and it can be seen that the peak mean value of $|\nabla c|$ is smaller for the water droplet cases in comparison to the corresponding premixed flame cases for both inertial and inertialess particles. This suggests that the flames with water droplets are thicker than the purely gaseous premixed flame, which is consistent with smaller laminar burning velocity for water loading than the unstrained laminar burning velocity of a stoichiometric premixed laminar flame (i.e. $S_b^{Y_W} < S_{b(\phi_g=1)} = S_{b(\phi_g=1)}^{Y_W=0}$) because the flame thickness scales as $\delta \sim \alpha_{T0}/S_{b(\phi_g=1)}$. This flame thickening is the strongest for the smallest droplets because of a decreasing trend of $S_b^{Y_W}$ with decreasing a_d/δ_{st} [6], as a result of stronger cooling effects owing to a higher evaporation rate in the case of smaller droplets.

The flame thickening with increasing droplet size weakens and the peak mean value of $|\nabla c|$ for initial $a_d/\delta_{st} = 0.04$ and 0.06 remain comparable (but slightly smaller) than the corresponding value in the gaseous premixed flame case. Fig. 6 reveals that the droplet inertia does not have a major influence on the mean variations of $\dot{\omega}_c \times \delta_{st}/(\rho_0 S_{b(\phi_g=1)})$ and $|\nabla c| \times \delta_{st}$ but the mean values of these quantities for inertialess droplets are slightly greater than those for inertial droplets. This is a consequence of a combination of smaller droplet number and smaller residence time within the flame for inertialess droplets and therefore the cooling effect associated with evaporation is relatively weaker in the inertialess droplets than in the case of inertial droplets. Although droplet inertia does not have a major influence on the results shown in Fig. 6, the droplet inertia plays a relatively more prominent role for the volume-integrated quantities (e.g. flame surface area and volume-integrated fuel reaction rate).

The values of the normalised flame surface area A_c/A_0 and A_T/A_0 for both the premixed and droplet cases are shown in Fig. 7 where the areas A_c and A_T are given by the volume-integrals $A_c = \int_V |\nabla c| dV$ and $A_T = \int_V |\nabla T| dV$ and A_0 is the flame surface area for the planar unstrained laminar premixed flame which, under the unity Lewis number condition, equals to $A_0 = \int_V |\nabla c|_L dV = \int_V |\nabla T|_L dV$. Fig. 7 shows that A_c values for the inertial droplet cases remain smaller than the corresponding value for the gaseous premixed flame cases, and the reduction of the flame surface area increases with decreasing a_d/δ_{st}.

It can be seen from Fig. 7 that values of A_c for the inertialess particles assume higher values than those in the case of inertial particles and for initial $a_d/\delta_{st} = 0.04$ and 0.06 cases, A_c values remain comparable to the gaseous premixed flame values

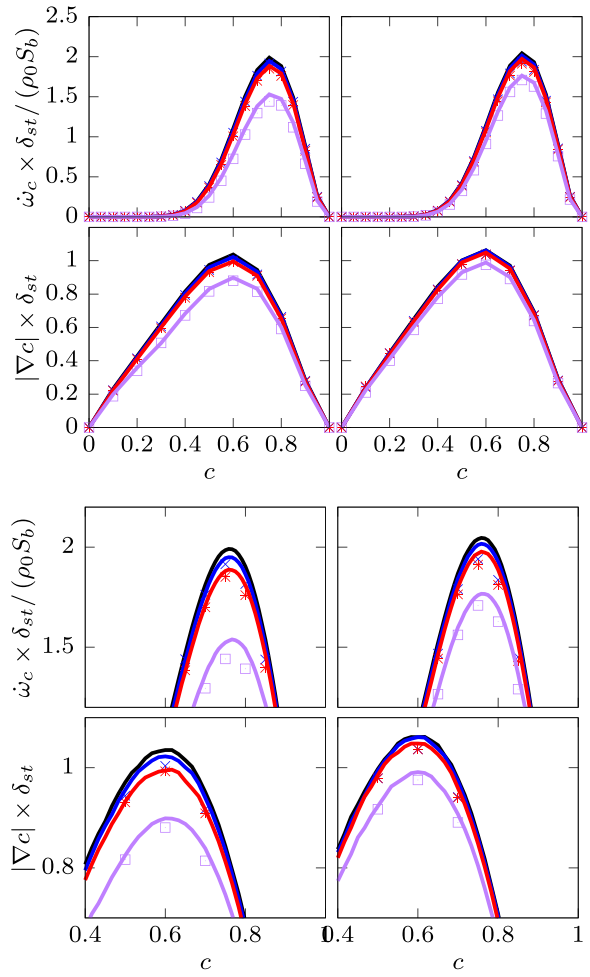

Fig. 6. Variations of $\dot{\omega}_c \times \delta_{st}/\rho_0 S_{b(\phi_g=1)}$ (1^{st} row and 3^{rd} row for the magnified view for the peak values) and $|\nabla c| \times \delta_{st}$ (2nd row and 4^{th} row for the magnified view for the peak values) conditional on c at $t/t_{chem} = 3$. Initial $u'/S_{b(\phi_g=1)} =$ 4.0 (1^{st} column) and 8.0 (2nd column) cases with inertial (markers) and inertialess (solid line) droplet cases with initial $a_d/\delta_{st} = 0.02$ (purple), 0.04 (red), 0.06 (blue) and purely premixed conditions (black solid line). (For interpretation of the references to color in this figure legend, the reader is referred to the web version of this article.)

but A_c in the initial $a_d/\delta_{st} = 0.02$ inertialess case remains slightly smaller than the premixed flame surface area. An increase in A_c for inertialess particles in comparison to inertial particles is consistent with the $|\nabla c|$ variation shown in Fig. 6 but differences in A_c between inertial and inertialess particles remain greater than the differences in mean values of $|\nabla c|$. As A_c is defined as $A_c = \int_V |\nabla c| dV$, it is not only $|\nabla c|$ but also the flame volume that affects A_c values. This suggests that the samples with high values of $|\nabla c|$ are more frequent in the inertialess droplet cases than in the case of inertial droplets.

Fig. 7 also shows that A_T for the inertial droplet case with initial $a_d/\delta_{st} = 0.06$ assumes higher values than the corresponding value for the gaseous premixed flame case for which $A_c = A_T$ due to the unity Lewis number assumption. However, A_T for the inertial droplet case with initial $a_d/\delta_{st} = 0.02$ remain marginally smaller than the corresponding value for the premixed flame. The A_T values for the inertial droplet case with initial $a_d/\delta_{st} = 0.04$ is almost the same as that of the gaseous premixed flame value. The cases with inertialess particles exhibit a higher value of A_T than that in the cases of the inertialess particles. It has already been demonstrated that a higher rate of evaporation for the smaller droplets acts to reduce the burned gas temperature (see Fig. 5), and this leads to a smaller magnitude of $|\nabla T|$ with decreasing a_d/δ_{st}. The smaller values of $|\nabla T|$ within the flame for initial $a_d/\delta_{st} = 0.02$ cases are principally responsi-

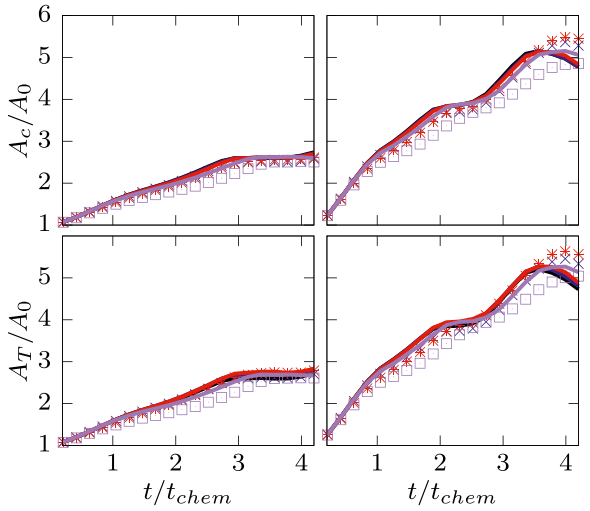

Fig. 7. Variations of normalised flame surface areas A_c/A_0 (1^{st} row) and A_T/A_0 (2nd row). Initial $u'/S_{b(\phi_g=1)} = 4.0$ (1^{st} column) and 8.0 (2nd column) cases with inertial (markers) and inertialess (solid line) droplet cases with initial $a_d/\delta_{st} =$ 0.02 (purple), 0.04 (red), 0.06 (blue) and purely premixed conditions (black solid line). (For interpretation of the references to color in this figure legend, the reader is referred to the web version of this article.)

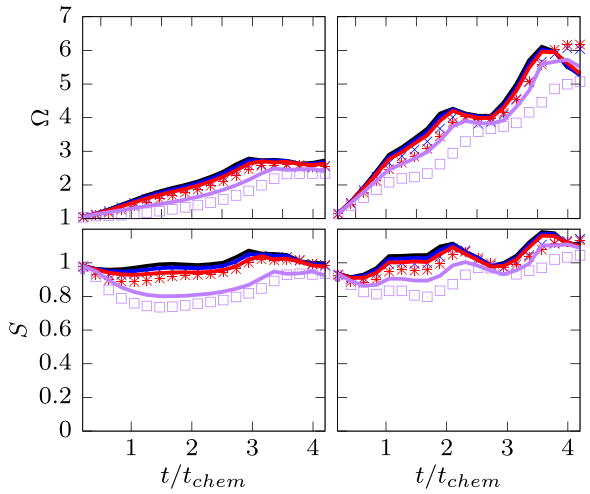

Fig. 8. Variations of $\Omega = \int_V |\dot{\omega}_F| dV/\left(\rho_0 Y_{F_{st}} A_0\right)$ (1^{st} row) and $S = \int_V \dot{\omega}_c dV/\left(\rho_0 S_{b(\phi_g=1)} A_c\right)$ (2nd row). Initial $u'/S_{b(\phi_g=1)} = 4.0$ (1^{st} column) and 8.0 (2nd column) cases with inertial (markers) and inertialess (solid line) droplet cases with initial $a_d/\delta_{st} = 0.02$ (purple), 0.04 (red), 0.06 (blue) and purely premixed conditions (black solid line). (For interpretation of the references to color in this figure legend, the reader is referred to the web version of this article.)

ble for smaller value of A_T than that in the premixed flame. By contrast, large droplets (e.g. initial $a_d/\delta_{st} = 0.06$ cases) pass through the flame before the completion of their evaporation in the burned gas and induce additional temperature gradient in the burned gas. Moreover, the water droplets induce additional wrinkling of T isosurfaces due to the extraction of latent heat (see Fig. 2). This gives rise to a higher value of A_T in the initial $a_d/\delta_{st} =$ 0.06 cases than that in the premixed flame. The effects of smaller values of $|\nabla T|$ within the flame and the temperature gradient within the burned gas along with droplet-induced T iso-surface wrinkling cancel each other for the inertial droplets with initial $a_d/\delta_{st} = 0.04$ and thus in this case A_T remains comparable to that of the premixed flame. The combination of the smaller extent of evaporation and smaller residence time acts to increase

$|\nabla T|$ within the flame for the cases with inertialess droplets in comparison to the cases with inertial droplets.

The effects of droplet inertia on $\dot{\omega}_c$, $|\nabla c|$, A_c and A_T (see Figs. 6 and 7) also affect the overall burning rate and the consumption rate of reactants per unit flame surface area, which are demonstrated in Fig. 8 where the variations of normalised fuel consumption rate $\Omega = \int_V |\dot{\omega}_F| dV/(\rho_0 Y_{F_{st}} A_0)$ and normalised reactants consumption rate per unit area $S = \int_V \dot{\omega}_c dV/\left(\rho_0 S_{b(\phi_g=1)} A_c\right)$ are shown for different droplet sizes for both inertial and inertialess particles. Fig. 8 shows that Ω and S decrease with decreasing a_d/δ_{st} for both inertial and inertialess particles, which is a consequence of small $\dot{\omega}_c$ values for small droplets (see Fig. 6). However, this cooling effect is weaker for inertialess droplets and therefore Ω values for these cases are greater than those in the case of inertial droplets.

The adverse effects of water loading on the burning rate for the cases considered here can also be substantiated from the values of S. A value of $S = 1.0$ indicates that the consumption rate of reactants per unit flame surface area remains the same as that of the laminar premixed flame. It can be seen from Fig. 8 that S remains almost equal to unity for the turbulent premixed flames, which is indicative of the validity of Damköhler's first hypothesis [14,23], and the reasons for the validity of Damköhler's first hypothesis for statistically planar turbulent premixed flames with unity Lewis number are discussed elsewhere [24] and thus are not repeated here. By contrast, S remains mostly smaller than unity for all droplet cases which is indicative of the smaller consumption rate of fuel than in the unstretched laminar premixed flame and therefore adverse effects of water loading on the burning rate in the cases considered here. Because of the stronger cooling effects for smaller droplets, the value of S decreases with decreasing a_d/δ_{st}. As the cooling effects are weaker for inertialess droplets, S assumes higher values for inertialess droplets than for inertial droplets.

This suggests that the reduction of the overall burning rate $\int_V |\dot{\omega}_F| dV$ (and also $\int_V \dot{\omega}_c dV$) with increasing water droplet diameter takes place at a higher proportion than that of the reduction in flame surface area A_c and the droplet inertia augments in this reduction in the burning rate. This suggests that the proper modelling of droplet inertia is important not only for multiphase aspects of the premixed flame-water droplet interaction but also is necessary for the purpose of capturing the correct flame structure for water droplet interaction with premixed flames.

4. Conclusions

The influence of water droplet inertia on the reaction zone structure, burned gas temperature, flame surface area and overall burning rate has been investigated for statistically planar stoichiometric n-heptane-air flames interacting with monosized water droplets using three-dimensional carrier phase DNS. Different initially mono-disperse droplet sizes have been considered for inertial and hypothetical inertialess liquid water droplets to isolate the effects of droplet inertia. It has been found that the cases with inertial droplets exhibit a higher residence time and greater extent of evaporation within the flame than those with inertialess droplets. This gives rise to the higher number density of droplets within the flame for the inertial droplet cases than in the corresponding inertialess droplet cases where the fluid velocity carries them from the unburned to the burned gas side with a short residence time. The higher number density of inertial droplets within the flame induces a greater extent of droplet-induced cooling than in the corresponding inertialess droplet cases, which leads to a thicker flame-front for inertial droplet cases than in the corresponding inertialess droplet cases. This also induces higher values of reactive scalar gradient within the flame and consequently greater flame surface area for inertialess droplets than in the case of inertial droplets. The combination of the cooling effect induced by the extraction of latent heat of water droplets (primary effect) and the reduction in reactant concentrations in the unburned gas (secondary effect) induce smaller overall burning rate and reactant consumption rate per unit flame surface area in the water droplet cases than in the gaseous premixed flame. However, this effect is weaker for inertialess droplets than for inertial droplets owing to the longer residence of inertial droplets within the flame. Therefore, inertial effects of droplets need to be properly addressed for the accurate modelling of both the two-phase nature of the flow field and the flame structure in the water spray interaction with premixed flames.

Declaration of Competing Interest

The authors declare that they have no known competing financial interests or personal relationships that could have appeared to influence the work reported in this paper.

Acknowledgments

JH gratefully acknowledges a postdoc fellowship of the German Academic Exchange Service (DAAD). NC acknowledges EPSRC (EP/R029369/1, EP/S025154/1) for computational and financial support. Funding by dtec.bw – Digitalization and Technology Research Center of the Bundeswehr, Project MORE, is also gratefully acknowledged.

References

[1] S. Lellek, Pollutant Formation in Premixed Natural Gas Swirl Flames with Water Injection, Technische Universität München, 2017 Ph.D. thesis.

[2] L. Fan, C.T. Chong, K. Tanno, D. McGrath, Y. Zheng, S. Hochgreb, Measurement of the effect of water droplets on strained laminar flames using two-phase PIV, Proc. Combust. Inst. 38 (2021) 3183–3192.

[3] G. Thomas, A. Jones, M. Edwards, Influence of water sprays on explosion development in fuel-air mixtures, Combust. Sci. Technol. 80 (1991) 47–61.

[4] K. Van Wingerden, B. Wilkins, The influence of water sprays on gas explosions. part 1: water-spray–generated turbulence, J. Loss Prevent. Proc. 8 (1995) 53–59.

[5] C. Nicoli, P. Haldenwang, B. Denet, Premixed flame dynamics in presence of mist, Combust. Sci. Technol. 191 (2019) 197–207.

[6] J. Hasslberger, G. Ozel-Erol, N. Chakraborty, M. Klein, S. Cant, Physical effects of water droplets interacting with turbulent premixed flames: a direct numerical simulation analysis, Combust. Flame 229 (2021) 111404.

[7] C.E. Polymeropoulos, Flame propagation in aerosols of fuel droplets, fuel vapor and air, Combust. Sci. Technol. 40 (1984) 217–232.

[8] J. Greenberg, Finite-rate evaporation and droplet drag effects in spherical flame front propagation through a liquid fuel mist, Combust. Flame 148 (2007) 187–197.

[9] M.A. Jog, P.S. Ayyaswamy, I.M. Cohen, Evaporation and combustion of a slowly moving liquid fuel droplet: higher-order theory, J. Fluid Mech. 307 (1996) 135–165.

[10] F. Atzler, F. Demoulin, M. Lawes, Y. Lee, N. Marquez, Burning rates and flame oscillations in globally homogeneous two-phase mixtures (flame speed oscillations in droplet cloud flames), Combust. Sci. Technol. 178 (2006) 2177–2198.

[11] M. Lawes, A. Saat, Burning rates of turbulent isooctane aerosol mixtures in spherical flame explosions, Proc. Combust. Inst. 33 (2011) 2047–2054.

[12] G. Ozel-Erol, N. Chakraborty, Inertial effects on globally stoichiometric spherically expanding turbulent flames propagating in Droplet-Laden mixtures, Proc. Combust. Inst. 38 (2021) 3379–3387.

[13] E. Fernández-Tarrazo, A.L. Sánchez, A. Linan, F.A. Williams, A simple one-step chemistry model for partially premixed hydrocarbon combustion, Combust. Flame 147 (2006) 32–38.

[14] G. Ozel-Erol, J. Hasslberger, M. Klein, N. Chakraborty, A direct numerical simulation analysis of turbulent v-shaped flames propagating into droplet-laden mixtures, Int. J. Multiphase Flow 133 (2020) 103455.

[15] M. Chaos, A. Kazakov, Z. Zhao, F.L. Dryer, A high-temperature chemical kinetic model for primary reference fuels, Int. J. Chem. Kinet. 39 (2007) 399–414.

[16] J. Réveillon, L. Vervisch, Spray vaporization in nonpremixed turbulent combustion modeling: a single droplet model, Combust. Flame 121 (2000) 75–90.

[17] A.P. Wandel, N. Chakraborty, E. Mastorakos, Direct numerical simulations of turbulent flame expansion in fine sprays, Proc. Combust. Inst. 32 (2009) 2283–2290.

[18] P. Schroll, A.P. Wandel, R.S. Cant, E. Mastorakos, Direct numerical simulations of autoignition in turbulent two-phase flows, Proc. Combust. Inst. 32 (2009) 2275–2282.

[19] P. Gualtieri, F. Picano, G. Sardina, C.M. Casciola, Clustering and turbulence modulation in particle-laden shear flows, J. Fluid Mech. 715 (2013) 134.

[20] D.H. Wacks, N. Chakraborty, E. Mastorakos, Statistical analysis of turbulent flame-droplet interaction: a direct numerical simulation study, Flow Turbul. Combust. 96 (2016) 573–607.

[21] G. Ozel Erol, J. Hasslberger, M. Klein, N. Chakraborty, A direct numerical simulation investigation of spherically expanding flames propagating in fuel droplet-mists for different droplet diameters and overall equivalence ratios, Combust. Sci. Technol. 191 (2019) 833–867.

[22] R. Sankaran, E.R. Hawkes, J.H. Chen, T. Lu, C.K. Law, Structure of a spatially developing turbulent lean methane–air bunsen flame, Proc. Combust. Inst. 31 (2007) 1291–1298.

[23] G. Damköhler, The effect of turbulence on the combustion rate in gas compounds, Z. Elktrochem. Angew. Proc. 46 (1940). CP4–CP4

[24] N. Chakraborty, D. Alwazzan, M. Klein, R.S. Cant, On the validity of Damköhler's first hypothesis in turbulent bunsen burner flames: a computational analysis, Proc. Combust. Inst. 37 (2019) 2231–2239.